Journal of Techniques, ISSN: 2708-8383, Vol. 8, No. 2, 2026, Pages 1-13
https://doi.org/10.51173/jt.v8i2.2915

JOURNAL OF TECHNIQUES

Journal homepage: http://journal.mtu.edu.iq

RESEARCH ARTICLE - ENGINEERING (MISCELLANEOUS)

Intelligent Adaptive PID Control for Ship Motion Using Radial Basis Function Artificial Neural Networks

Maha Yousif Hasan[1], Noor Q. Yousif[1], Mohammed K. Hamzah[1], Huthaifa Al-Khazraji[1], Amjad J. Humaidi[1], Farouk Zouari[2*]

[1]College of Artificial Intelligence Engineering, University of Technology-Iraq, Baghdad, Iraq

[2]University of Tunis Elmanar, Tunis, Tunisia

[*] Corresponding author E-mail: farouk.zouari@enit.utm.tn

Article Info.

Article history:

Received
06 March 2026

Revised
02 June 2026

Accepted
10 June 2026

Published
30 June 2026

Abstract

This study presents an intelligent adaptive PID controller based on Radial Basis Function neural network (PID–RBF) for motion control of a ship subjected to surge, heave, and pitch dynamics. The proposed controller adjusts PID parameters based on tracking errors to perfectly follow the desired trajectory and compensate for nonlinearity and uncertainty. The numerical simulations show that the proposed adaptive PID–RBF controller outperforms the traditional adaptive PID control in terms of accuracy and dynamic performance. The control efforts required by the proposed method have been considerably reduced. In the surge channel, the control energy is reduced from the value $9.58 \times 10^5$to 2.61×10^4, while there is a reduction in control energy from $3.95 \times 10^6$to 1.22×10^6 in the sense of pitch channel motion. In addition, the control signal from the proposed PID-RBF controller is smoother than that from the conventional control approach. This indicates that the proposed controller could reduce stress on the actuator and thereby keep it in a safe operating range by lowering the maximum control signal input. In addition, the results show that the proposed controller has better rejection capability and robustness than the conventional controller. The proposed PID–RBF controller demonstrates promising performance in the motion control of a ship across three motion channels (surge, heave, and pitch).

Publisher: Middle Technical University

Keywords: Adaptive PID Control; Radial Basis Function (RBF); Neural Network; Ship Dynamics; Motional Control; Tracking Accuracy; Tracking Performance.

1. Introduction

In recent years, ship motions have attracted considerable attention for control, especially with intelligent systems such as marine automation technologies. High-precision techniques must control parameter uncertainties and external interference, including high waves, bad weather, and ocean currents. Therefore, many control approaches seek to enhance their ability to handle complex, dynamic operating conditions without compromising the performance of the nonlinear system. To solve all issues, a range of control systems has been studied, including robust control, adaptive control, model predictive control (MPC), and AI-based strategies. Among these, smart control systems based on artificial neural networks (ANN) and machine learning (ML) strategies have shown great promise for addressing uncertainties and nonlinearities in ship motion performance. Radial Basis Function neural networks (RBF-NNs) have proven particularly popular due to their rapid convergence, universal approximation capacity, and applicability to real-time systems. These capabilities support adaptive behaviour and online learning, making them ideal for uncertain and dynamic maritime situations. Despite these technological advances, proportional-integral-derivative (PID) controllers are still commonly used in maritime and industrial applications due to their simplicity, quickness, and robustness [1–5]. It is predicted that almost 90% of industrial control systems still use PID-based approaches [6, 7]. As a result, current research has focused on improving PID reliability rather than replacing it entirely. Many research investigations [8–11] have presented optimal and adaptive PID-assisted ship control techniques. For instance, Al-Awad et al. [12] and T. Dlabač et al. [13] utilized particle swarm optimization (PSO) to tune PID parameters for improved transient response, while Nicolau [14] applied pole placement and symmetrical optimum methods for trajectory tracking under various reference inputs.

Nonlinear behaviors, parameter fluctuations, and external interference can all degrade the performance equality of traditional PID controllers. Constants and parameter variations are bounded according to operating conditions, resulting in reduced tracking accuracy and reduced rejection of external interference. These constraints underscore the need for more adaptable, intelligent control systems that perform well even under uncertain, harsh, and varying conditions.

Nomenclature & Symbols			
ANN	Artificial Neural Networks	K_i	Integral Parameter
ML	Machine Learning	K_d	Derivative Parameter
RBF	Radial Basis Function	τ_a	Adaptive PID Control Input
NN	Neural Network	$\dot{e}_i$	Tracking Error Derivative
PID	Proportional-Integral-Derivative	N	Number of Neurons
PSO	Particle Swarm Optimization	$\phi_i(e)$	Activation Function for Hidden Layer of RBF
RMSE	Root-Mean-Square Error	c_i	RBF Neuron Center
UUB	Uniform Ultimate Boundedness	ϵ	Small Constant to Avoid Division by Zero
DRR	Disturbance Rejection Ratio	W_p , W_i , W_d	Adaptive Weight Matrices
OS	Overshoot	η	Small Learning Rate
Ts	Settling Time	Δt	Simulation Time Step
Tr	Rise Time	τ_c	Control Torque Input
SSE	Steady-State Error	e_t	Error Between the Desired and Actual Ship Motion
IAE	Integrated Absolute Error	K_p	Proportional Parameter
τ	Adaptive Control Input	τ	Adaptive Control Input
q	Position Vector	q	Position Vector
$\dot{q}$	Velocity	$\dot{q}$	Velocity
$\ddot{q}$	Acceleration	Δt	Simulation Time Step
$D\,\dot{q}$	Nonlinear Damping Forces	τ_c	Control Torque Input
M_{sh}	Ship's Mass-Inertia Matrix	e_t	Error Between the Desired and Actual Ship Motion
$G(q)$	Gravity Compensation Vector	q_d	Desired Trajectory
τ_{max}	Maximum Control Input	A	Amplitude of the q_d
$M_{control,rbf}$	Maximum Control Input	$\dot{q}_d$	Desired Velocity

The integration of intelligent ML strategies and traditional PID control is a possible research topic. PID controllers are simple to design and robust, and neural networks have flexible capacity. Combination control strategies are developed by combining these two. This can dramatically enhance system effectiveness. Hence, in this work, a Radial Basis Function neural network-based intelligent adaptive PID controller (PID-RBF) for three-degree-of-freedom ship motion control is proposed. The suggested method allows continuous adjustment of the PID gains based on the tracked error rate, leading to better tracking accuracy, resilience, and interference rejection in a nonlinear shipping environment.

Such constraints drive the development of intelligent adaptive control techniques capable of dynamically adjusting controller parameters and ensuring stable performance under variable operating situations. To overcome these challenges, adaptive control solutions that use PID control methods have been created Åström and Hägglund (2006) developed error-driven tuning techniques for adaptive PID control, which are employed in the adaptive parameter update [15]. In this regard, Zhiping and Qiang [16] and Zhang et al. [17] proposed an adaptive self-regulation PID control strategy that accounts for unknown time-varying environmental disturbances and for variations in the ship's model parameters.

Alternatively, authors tend to develop new adaptive control methods combining the PID control with Artificial Neural Networks [18-21]. Ship dynamics are described by nonlinear equations and are affected by a wide range of external disturbances. Nonlinear and indeterminate features are also present in the external disruption component itself. As an outcome, specialized control techniques based on the Artificial Neural Network and the PID controller are designed to manage unknown variables and structures. Zhang, L et al. [22] and Hai [23] proposed a PID controller-based Artificial Neural Network (NN) where the NN is used to adjust the settings of the tuning parameters of the PID controller. The NN employs gradient descent to update its weights and ensure that the designed Artificial Neural Network can calculate the desired PID parameters. The use of standard Artificial Neural Networks to design adaptive PID controllers has limitations, including delayed adaptation, a lack of real-time parameter optimization, instability, and high computational cost, all of which lead to poor dynamic ship motion control. For effective and secure control of studies under various environmental circumstances. Hence, the effectiveness of traditional PID controllers can be severely degraded when dealing with nonlinear dynamics, unpredictability, and outside perturbations such as wind and waves. These constraints necessitate the development of more adapted and intelligent control techniques. To overcome all these problems, the proposed PID-RBF controller uses a Radial Basis Function neural network to adjust PID parameters in real time. Such an adaptive technique enables the controller to effectively respond to changing system dynamics, thereby improving tracking and optimization accuracy. A comparable technique was proposed by Yu et al. [24], which showed that an improved PID-RBF controller can enhance performance and overcome external disturbances. In this work, the PID parameters were adjusted periodically at each time instance, thereby reducing tracking errors using an RBF neural network. All these options increase response time while guaranteeing a stable response. Under nonlinear operating conditions, the combination of feedforward and gravity requirements concepts was integrated to improve the control performance. This integration enables the controllers to handle external interference more accurately. The aim of using the proposed method is to achieve greater simulation accuracy, reduced overshoot, lower tracking error rates, and improved robustness compared to traditional methods. Furthermore, the controller provides steady control signals while consuming less energy, thereby increasing overall efficiency. The benefits of the suggested method in all three motion directions, surge, heave, and pitch, are summarized by analyzing the performance using root-mean-square error (RMSE) and energy-dependent measures. All things considered, the adaptive PID-RBF controller provides a stable and effective solution for three ship motion control in challenging, uncertain marine environments by combining the ease of use and practicality of traditional PID control with the learning capabilities of neural networks.

2. Mathematical Model for Dynamic Ship System

For marine control systems to provide efficient steering and stability, ship characteristics must be precisely modeled. Based on the ship's basic physical properties, such as mass, nonlinear dynamics, kinetic damping, and gravity-related effects, this study develops an adaptive control

framework. The ship's motion is modeled as a nonlinear system that accounts for gravity compensation, damping forces, and inertia. The ship motion's nonlinear dynamics are characterized by the following equation [22].

$$\tau = M_{sh}\,\ddot{q} + D\,\dot{q} + G(q) \tag{1}$$

$\tau \in R^3$ is the adaptive control input vector, and $q = [q_1 \;\; q_2 \;\; q_3]^T$ denotes the position vector corresponding to surge, heave, and pitch motions. Also, in Eq. 1, the derivatives $\dot{q}$ represent the velocity, and $\ddot{q}$ represents the acceleration. $D\,\dot{q}$ represents the nonlinear damping forces, and M_{sh} is the ship's mass-inertia matrix, including added mass effects for surge, heave, and pitch, which is given by

$$M_{sh} = \begin{bmatrix} 50 & 0 & 0 \\ 0 & 200 & 0 \\ 0 & 0 & 500 \end{bmatrix} \tag{2}$$

The nonlinear damping matrix $D(\dot{q})$, which captures velocity-dependent hydrodynamic effects, is given by

$$D = \begin{bmatrix} 8 & 0 & 0 \\ 0 & 95 + 45\tanh(0.09\,|\dot{q_2}|) & 0 \\ 0 & 0 & 12 + 4.5|\dot{q_3}| \end{bmatrix} \tag{3}$$

while $G(q)$ is the gravity compensation vector term with an external disturbance, which takes gravity's restoring forces into effect, $G(q)$ is given by

$$G(q) = \begin{bmatrix} 0 & -1850\tanh\left(\frac{q_2}{9.5}\right) & 0 \end{bmatrix}^T \tag{4}$$

To ensure actuator safety and accurate operation, the control input has restrictions as follows: $\tau = \max(-\tau_{max}, \min(\tau_{max}, \tau))$, and the maximum control input range limits for the ship system (τ_{max}) is shown in Eq. 5:

$$\tau_{max} = [600 \;\; 6600 \;\; 180]^T \tag{5}$$

The system limits control inputs used to prevent excessive ship motion, expressed as 600 N (surge force), 6600 N (heave force), and 180 N (pitch force). These limitations ensure the control system operates within safe bounds by preventing excessive forces and torques that could cause instability or damage to the machine. Fig. 1 shows the ship's three-direction motions and their restrictions.

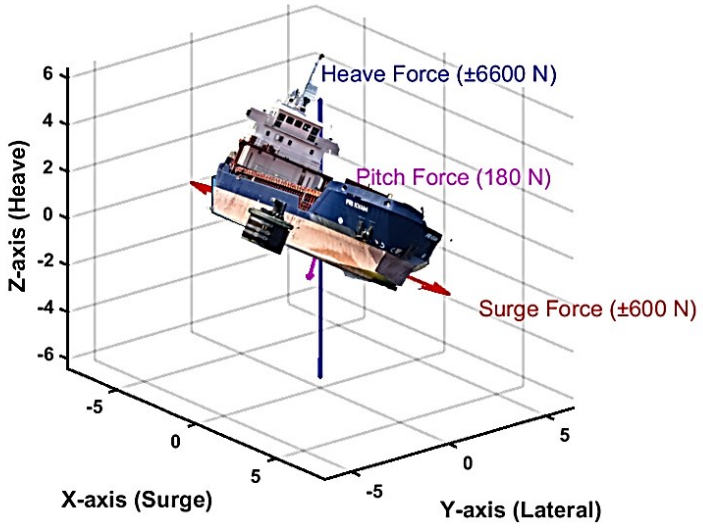

Fig. 1. The ship's three-direction motions and their restrictions

3. Controller Design

In this study, under difficult maritime conditions such as storms, high waves, and oceanic interference, these challenges were addressed using two control techniques developed to overcome them. Two types of controllers are introduced in this study. The main aim is to enhance the system's stability, including energy efficiency and tracking accuracy, which are assessed using metrics such as the root-mean-square error (RMSE). The first method relies on a traditional adaptive Proportional-Integral-Derivative (PID) controller that operates without the aid of artificial intelligence. By combining a Radial Basis Function (RBF) neural network with the PID controller, the second method proposes this structure and creates the PID–RBF strategy. Controller parameters are tuned adaptively in real time in this hybrid approach, thereby enhancing performance and reducing tracking errors and external interferences. In this study, a sine wave is used as a reference trajectory to provide a fair comparison between the two controller types. This reference trajectory q_d is used as a default to test the accuracy and efficiency of each control strategy.

A sine-wave trajectory was used to test both types of controllers used in this study. These types of trajectories used to represent the bad circumstances as a non-linear trajectory, which the ship may face when traveling in the ocean; therefore, the controller's role can see when to minimize the error between the actual trajectory of the ship's motions (surge, heave, and pitch) and the desired trajectory that must be traveled on it. The desired trajectory of q_d is defined by

$$q_d = A \sin(2\pi f t) \quad (6)$$

A is the amplitude of the q_d for three ship (surge, heave, and pitch) motions with effective outside interferences, $A = [2 \;\; 0.15 \;\; 5]^T$, f is the frequency rate for the q_d, and has a value (0.05 HZ). The desired velocity $\dot{q}_d(t)$, and acceleration $\ddot{q}_d(t)$ are derived.

$$\dot{q}_d(t) = \frac{d}{dt} q_d(t) = 2\pi f A \cos(2\pi f t) \quad (7)$$

$$\ddot{q}_d(t) = -(2\pi f)^2 A \sin(2\pi f t) \quad (8)$$

In this study, the outcomes of three ship motions for both controller types are simulated over 400 seconds, providing sufficient time to assess their effectiveness, stability, and accuracy. Using Eq. 1 to have,

$$\ddot{q} = M_{sh}^{-1} (\tau - D \dot{q} - G(q)) \quad (9)$$

M_{sh}^{-1} is the inverse of the ship's mass. To investigate the effect of external interference and the environment on the simulation of the outcomes for the ship's nonlinear system, one first needs to represent this system mathematically as given in Eq. 9, so that one can effectively use the controller to assess the accuracy and stability of this system from the simulation outcomes. Accordingly, the ship's velocity is updated as: $\dot{q}(t + \Delta t) = \dot{q}(t) + \ddot{q}(t)\Delta t$, and the position is updated as: $q(t + \Delta t) = q(t) + \dot{q}(t)\Delta t$. Δt represents the simulation time step. The nonlinear ship model, with the controller methods effective for this system, can be implemented in MATLAB. By tracking the error rate under the influence of the external environment, one can see how each controller mitigates instability in the ship system and how effectively it minimizes the error rate over time.

3.1. Traditional adaptive PID control

The traditional proportional-integral-derivative (PID) controller has been widely used in various control system applications, mainly due to its simplicity and robustness; however, its performance can degrade in the presence of nonlinearities and external disturbances, necessitating the development of advanced adaptive control techniques [25-29]. PID is a feedback control technique with three terms: proportional, integral, and derivative, that generates its control input law for any dynamic system. Its simplicity and efficiency make it a popular choice for controlli- to keep in mind that the adaptive method does not directly generate the PID settings. The controller parameters are not restricted to a specific range (e.g., ±1) and can vary within appropriate constraints, enabling effective adaptive tuning. Adaptive PID control input law ($\tau_a(t)$) for the ship dynamic system is given by

$$\tau_a(t) = \tau_c(t) + \text{Feedforward} + G_{correction} \quad (11)$$

Feedforward is a feedforward term: $\text{Feedforward} = M_{sh}\ddot{q}_d + D\dot{q}_d$, and $G_{correction} = \left[0 \quad -370 \tan^{-1}(\frac{\dot{q}_2}{9}) \quad 0\right]^T$, $G_{correction}$ is introduced to compensate for the gravitational restoring forces represented by $G(q)$ in the ship dynamics as expressed in Eq. 4.

Traditional adaptive PID controller parameters are updated with the control law based on tracking error $e_t(t)$ between the desired and actual ship motion, which can be defined as: $e_i(t) = q_d(t) - q(t)$, where $q_d(t)$ is a desired trajectory for the ship, and $q(t)$ is the actual trajectory motion for the ship (surge, heave, and pitch). $\dot{e}_i(t)$ is the tracking error derivative given by

$$\frac{de_t(t)}{dt} = \dot{e}_i(t) = \dot{q}_d(t) - \dot{q}(t) \quad (12)$$

Using Eq. (11), one can have

$$\tau_a(t) = \tau_c(t) + M_{sh}\ddot{q}_d + (1.05 \times D\dot{q}_d) + \left[0 \quad -370 \tan^{-1}\left(\frac{\dot{q}_2}{9}\right) \quad 0\right]^T \quad (13)$$

To find the adaptive PID (K_p , K_i, and K_d) parameters, calculations can use simple error-driven rules, which are: $K_p = K_p + |e(t)|$, $K_i = K_i + |\int e(t)\, dt|$, $K_d = K_d + |\dot{e}(t)|$. These rules are used to update adaptive PID parameters dynamically.

3.2. Adaptive PID with RBF-based ANN control

Applications of Artificial Neural Network principles to enhance system performance can be observed across various fields. To overcome the limitations of classical PID controllers, several hybridizations between classical PID and Artificial Neural Networks have been developed [29-32]. In this context, a proportional, integral, and derivative with radial basis function Artificial Neural Network (PID-RBF) controller is proposed to enhance the ship's three motions under adverse weather and sea conditions by minimizing tracking errors. The PID-RBF controller consists of an Artificial Neural Network. PID-RBF control uses a Radial Basis Function (RBF) and a multilayer Artificial Neural Network (ANN) to adjust PID parameters for optimal performance dynamically. In the PID-RBF control system, by optimizing control parameters, the Artificial Neural Network is trained to reduce steady-state error and improve adaptability. It employs a Gaussian activation function based on real-time tracking errors used for nonlinear systems [33, 34]. The RBF-N. N updates dynamic PID parameters effectively due to its excellent interpolation capabilities, thereby accelerating the training process. The RBF-N. N activation of the hidden layers for the RBF-N. N has the following form, as given by:

$$\phi_i(e) = e^{\left(\frac{-(\|e - c_i\|)^2}{2\sigma^2}\right)} \quad (14)$$

$\phi_i(e)$ is the RBF, c_i: is the RBF neuron center for the spacing between parameters data speared with the change in the ship's motion, and, σ is the spread parameter (width of the Gaussian function) equal to (1.4). The normalized RBF activation form is given by:

$$\Phi_i(e) = \frac{\phi_i(e)}{\sum_{i=1}^{N} \phi_i(e) + \epsilon} \quad (15)$$

ϵ is a small constant to avoid division by zero equal to (10^{-6}), and (N) is the number of neurons of the RBF-N.N function. Twenty-five RBF neurons have been installed for the preparation of Gaussian activation functions. The Radial Basis Function Artificial Neural Network (RBF-NN) structure for adaptive PID parameter tuning can be shown in Fig. 2.

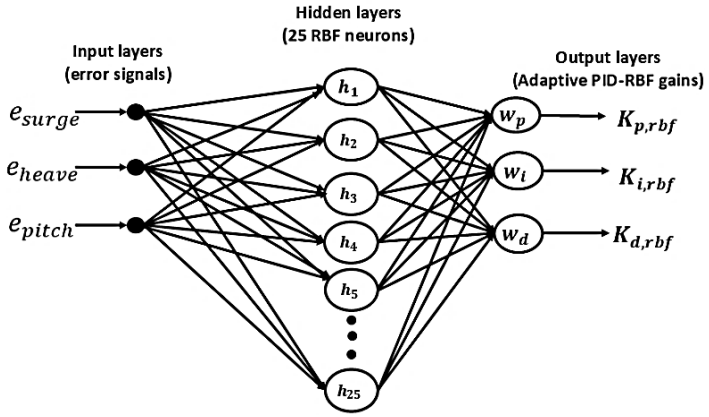

Fig. 2. The (RBF-N. N) structure for updating the adaptive PID parameter

The final control input formula for the adaptive PID-RBF control system becomes as given by:

$$\tau_{rbf}(t) = K_{p,rbf}e_t(t) + K_{i,rbf}\int e_t(t)\,dt + K_{d,rbf}\dot{e}_t(t) + M_{sh}\ddot{q}_d + (1.05 \times D\dot{q}_d) + \left[0 \quad -370\tan^{-1}\left(\frac{\dot{q}_2}{9}\right) \quad 0\right]^T \tag{16}$$

Adaptive PID-RBF has ($K_{p,rbf}$, $K_{i,rbf}$, and $K_{d,rbf}$) parameter calculations, used with bounded constraints, which are crucial in unpredictable environments. They balance stability, adaptability, and intelligence, using RBF outputs to prevent large increases [35]. The adaptive PID-RBF parameters are dynamically computed from these rules and are given by the following set of equations:

$$K_{p,rbf} = \begin{cases} 88 & \sum W_p\ \Phi_i(e) < 88 \\ \sum W_p\ \Phi_i(e) & 88 \le \sum W_p\ \Phi_i(e) \le 98 \\ 98 & \sum W_p\ \Phi_i(e) > 98 \end{cases} \tag{17}$$

$$K_{i,rbf} = \sum \frac{W_i\ \Phi_i(e)}{(1+1.2|e_2|)} \tag{18}$$

$$K_{d,rbf} = \begin{cases} 90 & \sum W_d\ \Phi_i(e) < 90 \\ \sum W_p\ \Phi_i(e) & 90 \le \sum W_d\ \Phi_i(e) \le 98 \\ 98 & \sum W_d\ \Phi_i(e) > 98 \end{cases} \tag{19}$$

W_p , W_i , W_d : are the adaptive weight matrices of the adaptive PID-RBF control. The parameter constraints in Eqs. 17, 18, and 19 are introduced to ensure that the adaptive parameters remain within predefined practical limits. The adaptive weight matrices are instantly updated within the specified constraints in response to changes in the ship system error, rather than being fixed. These updates enable the controller to handle changes in external interference and a harsh environment, and Fastly helps stabilize the system. The control input is calculated as expressed in Eq. 1, but Adaptive weight matrices of the adaptive PID-RBF control can be updated by using an adaptive gradient descent formula given by the following equations:

$$\Delta W_p = W_p + (\eta(\Phi_i(e)e^T) - (\lambda \times W_p)) \tag{20}$$

$$\Delta W_i = W_i + (\eta(\Phi_i(e)\int e^T\,dt) - (\lambda \times W_i)) \tag{21}$$

$$\Delta W_d = W_d + (\eta(\Phi_i(e)\dot{e}^T) - (\lambda \times W_d)) \tag{22}$$

η is the small learning rate value (η = 0.05) to guarantee silky convergence and prevent extreme oscillation, and($\lambda = 0.002$) is the decay factor, which is used to prevent uncontrolled adaptation by avoiding large increases in weight growth. The adaptive PID-RBF controller, illustrated in Fig. 3, uses an RBF-NN to adjust PID parameters ($K_{p,rbf}$, $K_{i,rbf}$, and $K_{d,rbf}$) for motion-shipped control, thereby enhancing real-time adaptability. It also adjusts parameters based on trajectory errors to achieve smooth, effective motion control.

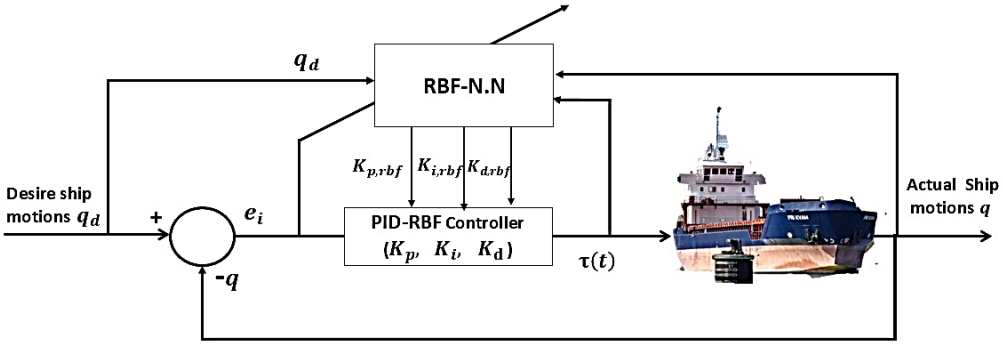

Fig. 3. Block diagram of the adaptive PID-RBF control system

3.3. Lyapunov-based stability analysis

The adaptive PID-RBF controller provides system stability via Lyapunov stability analysis. This control system utilizes a Lyapunov-based architecture to provide closed-loop stability. The concepts of adaptive learning in the Radial Basis Function (RBF) Artificial Neural Network ensure that the tracking error converges asymptotically to zero while keeping system signals within bounds. A Lyapunov function is developed based on tracking and weight estimation errors, and its time derivative is demonstrated to be negative definite, proving the closed-loop system's global asymptotic stability. The evidence of Lyapunov stability requires establishing the existence of a Lyapunov function $V(e,w) \succ 0$. Therefore, it is positive definite for $\forall e \neq 0$, except at the origin $V(0) = 0$, Then the system is globally asymptotically stable through time if its derivative $\dot{V} \prec 0$, $\forall e \neq 0$ except at the origin $\dot{V}(0) = 0$, Lyapunov's typical function is defined for the proposed ship control motion, given by:

$$V(e,w) = \frac{1}{2}e^T M_{sh} e + \frac{1}{2}\sum_{i=1}^{n}\left(W_p{}^T W_p + W_i{}^T W_i + W_d{}^T W_d\right) \quad (23)$$

$$V(e,w) \succ \frac{1}{2}e^T M_{sh} e + \frac{1}{2}\left(\|W_p\|^2 + \|W_i\|^2 + \|W_d\|^2\right) \quad (24)$$

The function remains positive definite; M_{sh} is positive definite because its norms are squares. The e term ensures unbounded, where for $\| e \| \to \infty for \boldsymbol{V} \to \infty$, therefore; $V(e,w)$ is positive definite, which means $(e,w) > 0$, for $\forall e \neq 0$. Now, for taking the time derivative $V(e,w)$, one can obtain

$$\dot{V} = e^T M_{sh}\dot{e} + (W_p{}^T \dot{W_p} + W_i{}^T \dot{W_i} + W_d{}^T \dot{W_d}) \quad (25)$$

Now, $\dot{W_p} = (\eta(\Phi_i(e)e^T) - (\lambda \times W_p))$, $\dot{W_i} = (\eta(\Phi_i(e)\int e^T dt) - (\lambda \times W_i))$, and $\dot{W_d} = (\eta(\Phi_i(e)\dot{e^T}) - (\lambda \times W_d))$ can use these equations for substituting them in the adaptive PID-RBF control equation (24) to get the following equations;

$$\dot{V} = e^T M_{sh}\dot{e} + W_p{}^T((\eta(\Phi_i(e)e^T) - (\lambda \times W_p)) + W_i{}^T(\eta(\Phi_i(e)\int e^T dt) - (\lambda \times W_i)) + W_d{}^T(\eta(\Phi_i(e)\dot{e^T}) - (\lambda \times W_d))) \quad (26)$$

$$\dot{V} \prec e^T M_{sh}\dot{e} + \eta(W_p{}^T + W_i{}^T + W_d{}^T)\Phi_i(e)e^T - \lambda(\|W_p\|^2 + \|W_i\|^2 + \|W_d\|^2)) \quad (27)$$

For η , $\lambda \succ 0$, and under bounded $\Phi_i(e)$, one can analyze the last Eq. 27 to a conclusion: the terms η, λ are positive definite parameters. Also, $\Phi_i(e)$, is positive definite and does not present an instability factor effect, since $\dot{V} \prec 0$. According to the Lyapunov analysis described in Eq. 27, the derivative of the Lyapunov function is negative semi-definite for restricted adaptation rules and outside influences. As a result, the closed-loop system satisfies the Uniform Ultimate Boundedness (UUB) condition, which guarantees that all system signals, including tracking errors and adaptive parameters, remain bounded over time. The proposed PID–RBF controller employs a Radial Basis Function neural network to adjust control parameters dynamically, enabling effective compensation of nonlinearities and external disturbances in ship motion dynamics. As a result, the trajectory tracking errors converge to a neighborhood around zero rather than asymptotically approaching zero, which is compatible with practical adaptive control systems operating under uncertain conditions. The proposed control technique is the best option for controlling ship motion instantaneously in nonlinear dynamic systems and uncertain marine environments, as it analyzes the ship system's outcomes and results show it maintains strong, dependable performance in the face of external disruptions.

4. Simulation Results and Discussion

In this section, MATLAB simulation results are presented for a ship system under high winds, strong waves, and other adverse conditions it may encounter during ocean travel. MATLAB simulation results are produced for both controller types used in this study. The first type of controller is the traditional PID controller, and the second is the proposed PID-RBF controller. Using the simulation results for both controller types, we can analyze which is the best option for dealing with the nonlinear ship dynamic system with high accuracy and a lower tracking error rate. Also, from these results, we can assess the robustness of each controller type using the root-mean-square error (RMSE) and the Disturbance Rejection Ratio (DRR). These terms are useful for assessing the effectiveness, the ability to track error rates, and the energy efficiency of ship system properties under these circumstances for each controller type. Specifically, the MATLAB software was used to simulate the traditional adaptive PID controller over 400 seconds. Its effects in these simulation results can directly illustrate the adaptive PID controller. Therefore, the adaptive PID controller shows good tracking accuracy with reduced error rates across the three ship motions (surge, heave, and pitch), but its performance does not reach optimal levels. This reduction led to a notable decrease in disturbance levels during actual trajectory tracking. Fig. 4 compares three-directional ship motion tracking between the Adaptive PID and PID-RBF control methods.

After adding the adaptive PID-RBF control to the ship dynamic system, the results showed improvements. From the MATLAB simulation, it was observed that the adaptive PID-RBF control significantly reduced the final error for each directional motion type (surge, heave, and pitch) in the ship dynamic system over a 400-second simulation. This reduction led to a notable decrease in disturbance levels during actual trajectory tracking. The simulation results show that the proposed control mechanism improves system stability and significantly reduces overshoot. The RBF-NN-based tuning process enables improved real-time reaction to disturbances. Fig. 4 shows the three-directional ship motions tracking comparison of the Adaptive PID and Adaptive PID-RBF control methods' response.

Evaluation of the performance of each control method type, then comparing the results for the conventional Adaptive PID controller with the Adaptive PID-RBF control by checking performance metrics by using the metric RMSE to evaluate the performance of each controller [36],

$$\mathrm{RMSE_i} = \sqrt{\frac{1}{\mathrm{N}}\sum_{\mathrm{i=1}}^{\mathrm{N}}\left(\mathrm{q_d(t_i)} - \mathrm{q(t_i)}\right)^2} \quad (28)$$

i: means each ship motion type (surge, heave, and pitch), and N is the total number of times the speed. Pitch, heave, and surge motions of ship types are calculated using RMS and normalized RMSE metrics to evaluate the controller's performance. Fig. 4 shows the three-directional ship motions tracking comparison of the Adaptive PID and adaptive PID-RBF control methods' response.

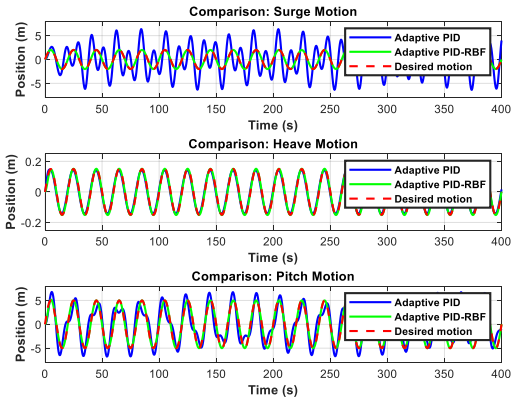

Fig. 4. A comparison of Adaptive PID and Adaptive PID- RBF control methods

The final RMSE comparison as bar values the two control methods for each ship's directional motion for the two methods as shown in Fig. 5. The RMSE results from Fig. 5 are detailed as shown in Table 1, which demonstrates the significant adjustments made by adding adaptive PID-RBF control into the ship dynamic system, resulting in a notable improvement in disturbance reduction and system performance for each ship motion type. Lower RMSE values indicate that the PID-RBF controller has improved trajectory-tracking accuracy. The adaptive PID-RBF controller is a viable option for ship motion control, as it effectively reduces tracking errors and adapts to changing motion conditions. Table 1 allows us to represent all the changes shown in Fig. 5 mathematically.

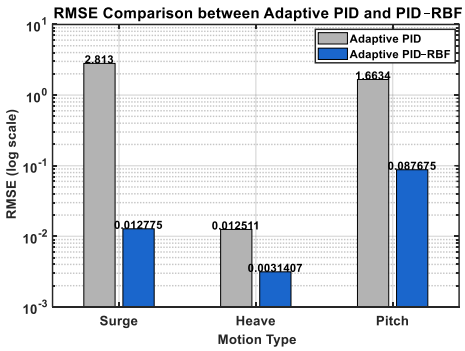

Fig. 5. Final RMSE comparison

The improvement ratio can be found from the RMSE for both types of controllers using Eq. 29;

$$\text{Improvement ratio } \% = \frac{\text{RMSE}_{\text{PID}} - \text{RMSE}_{\text{PID-RBF}}}{\text{RMSE}_{\text{PID}}} \times 100 \quad (29)$$

From Table 1, it can be observed that the RMSE results values for the adaptive PID-RBF control method: RMSE for Pitch motion is 0.09456, mean improvement from the adaptive PID control is 99.55 %, RMSE for Heave motion is 0.014943, mean improvement from the adaptive PID control 74.99 %, and RMSE for Surge motion is 0.013039, mean improvement from the adaptive PID control is 94.73 %.

Table 1. RMSE of Adaptive PID and PID- RBF control methods

Motion Type	RMSE		
	Traditional Adaptive PID	PID-RBF	Improvement (%)
Surge	2.813	1.28×10^{-2}	99.55 %
Heave	1.25×10^{-2}	3.14×10^{-3}	74.99 %
Pitch	1.6634	8.77×10^{-2}	94.73 %

4.1. Time-domain analysis

To quantitatively evaluate the transient and steady-state behaviour, standard time-domain metrics were computed, including overshoot (OS), settling time (Ts), rise time (Tr), and steady-state error (SSE). Beyond simply viewing simulation outcomes graphically, these performance measurements provide an analysis of the operating characteristics of each controller type. Essential time-dependent parameters, such as Ts, OS, Tr, and SSE, are compared for the proposed Adaptive PID–RBF controllers and the traditional adaptive PID across three ship motions (surge, heave, and pitch) in Table 2.

Table 2. Time-Domain Metrics

Motion Type	Controller Type	OS %	Ts(s)	Tr(s)	SSE
Surge	Adaptive PID	237.22	0.000	3.402	2.4757
	Adaptive PID-RBF	0.51501	0.072	2.979	60.18×10^{-3}
Heave	Adaptive PID	14.466	0.000	2.286	0.0156
	Adaptive PID-RBF	1.9139	0.072	3.618	11.11×10^{-3}
Pitch	Adaptive PID	62.317	0.000	3.501	1.6703
	Adaptive PID-RBF	5.0605	0.072	3.492	17.21×10^{-3}

The outcomes show that the traditional adaptive PID controller has high OS, especially during surge motion (237.22%), followed by heave motion (14.47%) and pitch motion (62.31%). The outcomes show that the transient behavior is weak and the damping capability is reduced. On the contrary, the proposed Adaptive PID-RBF controller can significantly reduce the OS to 0.51%, 1.91%, and 5.06% in surge, heave, and pitch motion, respectively. All these outcomes show that the damper metric is improved. The system stability is improved. The second outcome (Ts) shows an unreasonable value of 0.000 s for the traditional adaptive PID controller. Still, one can see that Ts is equal to 0.072 s with the proposed PID–RBF controller, as indicated by the ship system becoming faster and more stable simultaneously across three ship motions. The outcome Tr shows that the two controllers are relatively similar, but only slight differences are observed in the surge motion for the PID-RBF method: 2.979 s versus 3.402 s. This small difference shows that the proposed PID-RBF controller method achieves perfect tracking with greater accuracy for the ship's nonlinear system. The last outcome in this section is SSE, which showed a clear reduction in value under the proposed controller types. So, SSE values for the traditional PID control are equal to 2.4757 in surge, 0.0156 in heave, and 1.6703 in pitch. While SSE values for the proposed PID-RBF control are equal to 0.06018 in surge, 0.0111 in heave, and 0.01721 in pitch. These outcomes demonstrate that the proposed controller achieves the best SSE with approximately zero tracking error. Overall, the results clearly demonstrate that the Adaptive PID-RBF controller exceeds the traditional adaptive PID in terms of dynamic response. The suggested approach maintains faster settling and rise times while drastically lowering overshoot and steady-state error in all motion directions. These outcomes validate the enhanced transient stability and accuracy attained by the PID-RBF controller's neural adaptation mechanism.

4.2. Energy efficiency analysis

Comparing the results for the conventional Adaptive PID controller with the Adaptive PID-RBF control by checking energy efficiency ($E_{fficiency}$) performance metrics by calculating Energy consumption for each type of controller by using the following equations;

$$E_{consumed,i} = |\tau_{max,i}(t) \times RMSE_i| \tag{30}$$

$$E_{eficiency,i} = 1/E_{consumed,i} \tag{31}$$

The final Energy efficiency comparison values the two control methods for each ship's directional motion, as shown in Fig. 6. Table 3 summarizes the mathematical changes shown in Fig. 6.

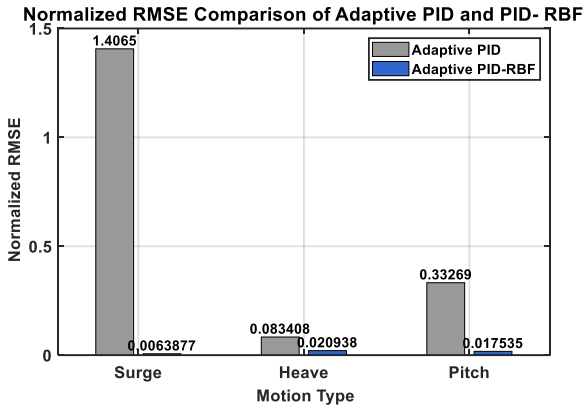

Fig. 6. Energy efficiency comparison

Energy efficiency means higher values are better values. The results of the $E_{fficiency}$ are shown in Fig. 7 and detailed in Table 3, which demonstrate the improvement in energy consumption and system performance achieved by adding Adaptive PID-RBF control for each ship motion type. Can find the improvement factor from energy efficiency from both types of controllers using Eq. 32;

$$\text{Improvement factor } \% = \frac{E_{efficiency,PID-RBF} - E_{efficiency,PID}}{E_{efficiency,PID}} \times 100 \tag{32}$$

From Table 3, the traditional Adaptive PID control achieves substantial energy efficiency $E_{efficiency}$ parameters, with values of approximately 7.1×10^{-4} in surge, 1.211×10^{-2} in heave, and 3.34×10^{-3} in pitch, without any improvement. In contrast, the proposed Adaptive PID-RBF control achieves substantial $E_{fficiency}$ parameters, with values of approximately 1.5656×10^{-1} in surge, 14.824×10^{-2} in heave, and 3.34×10^{-3} in pitch. From these results, we can clearly see improvements in the proposed Adaptive PID-RBF control, achieving substantial energy efficiency gains of approximately 22050% in surge, 298% in heave, and 1797% in pitch. The Adaptive PID-RBF control has a significantly higher $E_{efficiency}$, meaning it is much more energy-efficient than the Adaptive PID controller.

Table 3. Energy Efficiency of Adaptive PID and Adaptive PID- RBF control methods

Motion Type	$E_{eficiency}$		
	Traditional adaptive PID	Adaptive PID-RBF	Improvement factor (%)
Surge	7.1×10^{-4}	1.5656×10^{-1}	22050 %
Heave	1.211×10^{-2}	4.824×10^{-2}	298 %
Pitch	3.34×10^{-3}	6.337×10^{-2}	1797%

4.3. Control Effort and actuator smoothness analysis

In this section, the Control Effort and Actuator Smoothness Analysis are discussed from these outcomes. To elucidate the influence of the actuating mechanism wear, performance, and the long-term reliability of the ship's nonlinear system. The control energy ($E_{control}$) for the adaptive PID controller is defined by using the formula given by Eq. 33;

$$E_{control} = \int_0^T \tau(t)^2 \, dt \tag{33}$$

and the control energy ($E_{control,rbf}$) for the adaptive PID-RBF control is defined by using the formula given by Eq. 34;

$$E_{control,rbf} = \int_0^T \tau_{rbf}(t)^2 \, dt \tag{34}$$

The final control energy comparison values the two control methods for each ship's directional motion. Table 4 allows for conveyinprovides a mathematical summary in all Fig. 8 mathematically.

The control smoothness index ($S_{control}$) for the adaptive PID controller is defined by using the formula given by Eq. 35;

$$S_{control} = \int_0^T \left(\frac{d\tau(t)}{dt}\right)^2 \, dt \tag{35}$$

The control smoothness index ($S_{control,rbf}$) for the adaptive PID-RBF controller is defined by using the formula given by Eq. 36;

$$S_{control,rbf} = \int_0^T \left(\frac{d\ \tau_{rbf}(t)}{dt}\right)^2 \, dt \tag{36}$$

The control smoothness index comparison values the two control methods for each ship's directional motion, as shown in Fig. 7. Table 4 provides a mathematical summary of all the changes in Fig. 7. The Control smoothness index response is normalized in relation to the reference amplitude; thus, values greater than unity indicate overshoot relative to the desired outcome trajectory. The maximum control input ($M_{control}$) is also reported to evaluate actuator utilization for the adaptive PID controller, which is defined by using Eq. 37;

$$M_{control} = \max_{t\epsilon[0,T]} | \ \tau(t) \ | \tag{37}$$

The maximum control input ($M_{control,rbf}$) is also reported to evaluate actuator utilization for the adaptive PID-RBF controller, which is defined by using the formula given in Eq. 38;

$$M_{control,rbf} = \max_{t\epsilon[0,T]} | \ \tau_{rbf}(t) \ | \tag{38}$$

The maximum control input comparison values for the two control methods for each ship's directional motion are shown in Fig. 9. Table 4 summarizes all the changes mathematically. Table 4. Quantitative control-effort metrics (E, S, M) for Adaptive PID and Adaptive PID-RBF controllers across three ship motion modes.

From Table 4, in terms of control energy ($E_{control}$) for the adaptive PID control to the control energy ($E_{control,rbf}$) for the adaptive PID-RBF control is significantly reduced from 9.58×10^5 to 2.61×10^4 (surge), and from 3.95×10^6 to 1.22×10^6 (pitch). The terms of the control smoothness index ($S_{control}$) for the adaptive PID control are the same as the control smoothness index ($S_{control,rbf}$). The adaptive PID-RBF control is reflected by a reduction in the smoothness index from 3.59×10^5 to 5.07×10^3 (surge), and from 1.16×10^6 to 1.33×10^5 (pitch). The terms of the maximum control input ($M_{control}$) for the adaptive PID control to the maximum control input ($M_{control,rbf}$) for the adaptive PID-RBF control are significantly reduced from 99.29 to 61.81 (surge), and from 180.00 to 162.74 (pitch). The results show that adaptive PID-RBF control consistently requires less control effort and produces smoother actuation than conventional adaptive PID control. In surge motion, the proposed controller reduces total control energy from 9.58×10^5 to 2.61×10^4, a reduction of approximately 97%, and improves smoothness by more than 98%. Similarly, in pitch motion, adaptive PID-RBF control lowers the control energy by approximately 69% and smoothness by approximately 89%, while also reducing the peak actuator demand from 180 to 162.7. For heave motion, the overall energy consumption is similar between the two methods. Still, adaptive PID-RBF control achieves a smoother response (approximately 51% improvement in smoothness) and significantly reduces the maximum input demand (approximately 61%). The results of this study demonstrate that the adaptive PID-RBF control method improves the track precision, promotes safer, more energy-efficient control procedures, reduces operator fatigue, and improves overall system reliability.

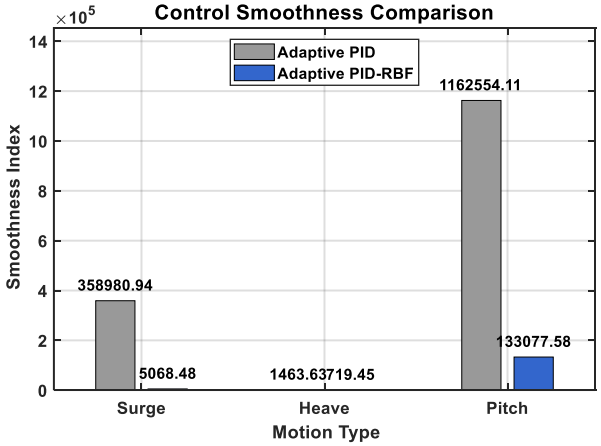

Fig. 7. Smoothness index comparison

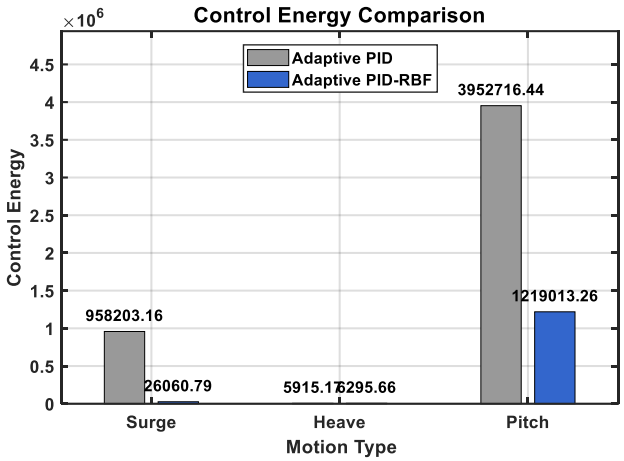

Fig. 8. Control energy comparison

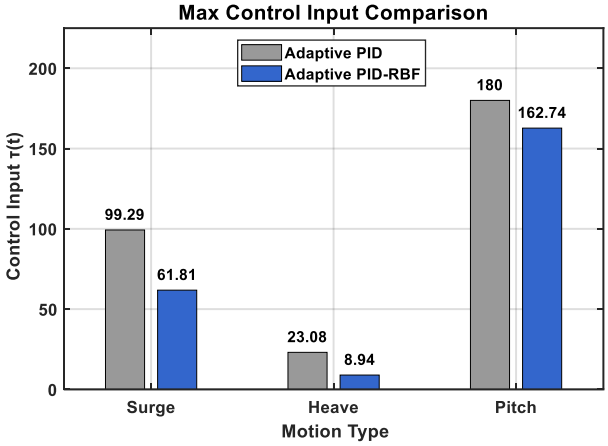

Fig. 9. Maximum control input comparison

Table 4. Control energy metrics

Evaluation Metric	Motion Type		
	Surge	Heave	Pitch
$E_{control}$	9.58×10^5	5.92×10	3.95×10^6
$E_{control,rbf}$	2.61×10^4	6.30×10^3	1.22×10^6
$S_{control}$	3.59×10^5	1.46×10^3	1.16×10^6
$S_{control,rbf}$	5.07×10^3	7.19×10^2	1.33×10^5
$M_{control}$	99.29	23.08	180.00
$M_{control,rbf}$	61.81	8.94	162.74

4.4. Integral absolute error and disturbance rejection

Additional performance metrics were considered to evaluate the resiliency and accuracy rate of the proposed controller under outside interference, including the Integrated Absolute Error (IAE) and the Disturbance Rejection Ratio (DRR_i). These metrics are defined by Eq. 39;

$$IAE = \int_0^T | (e_i(t)) | dt \tag{39}$$

$$DRR_i = \frac{\sqrt{\int_0^T |e_i(t)|^2 dt}}{\sqrt{\int_0^T |d_i(t)|^2 dt}} \tag{40}$$

The DRR_i is the ratio between the tracking error ($e_i(t)$) and the disturbance energy $d_i(t)$ on three ship motions (surge, heave, or pitch), a normalized measure of the control's ability to attenuate disturbances [37]. The simulation results in Fig. 10 and Fig. 11, respectively, for IAE and DRR_i Performance analysis show a considerable reduction in the performance measures (IAE and DRR_i) for the Adaptive PID-RBF control compared to the conventional Adaptive PID control. Table 5 presents all the changes in Figs. 10 and 11 mathematically.

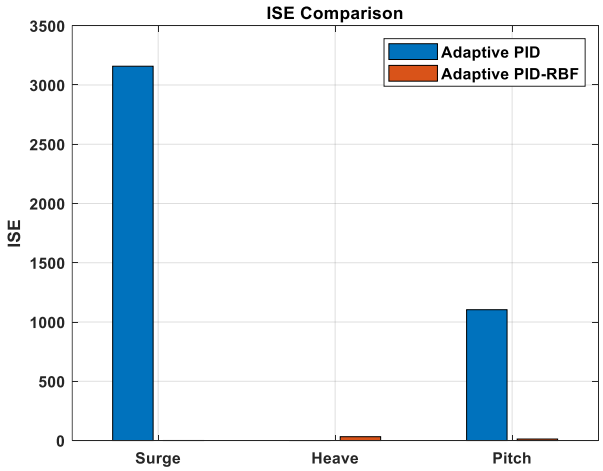

Fig. 10. IAE performance analysis comparison

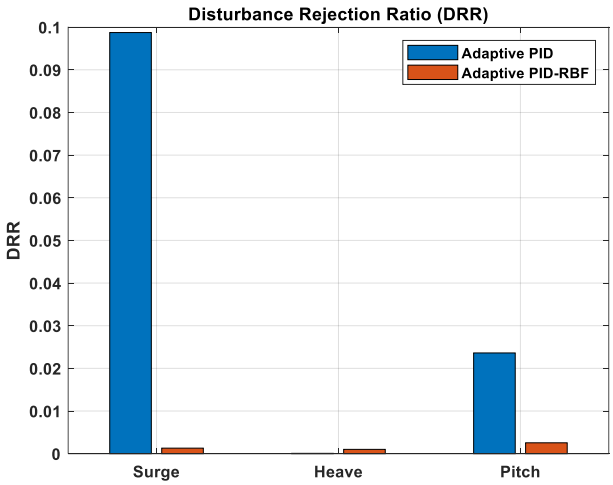

Fig. 11. DRR performance analysis comparison

Table 5. Performance analysis metrics

Evaluation Metric	Motion Type		
	Surge	Heave	Pitch
IAE PID	992.2332	7.0689	581.2013
IAE PID-RBF	0.5424	32.3221	12.8149
DRR PID	0.0987	0.0001	0.0236
DRR PID-RBF	0.0013	0.0010	0.0025

From Table 5, the results show a significant improvement in overall tracking accuracy for the adaptive PID-RBF control in two of the three ship motion types. In the surge motion, the *IAE* is reduced from 992.23 (adaptive PID) to 11.24 (adaptive PID-RBF), indicating a significant improvement in trajectory tracking under nonlinear dynamics and external disturbances. Similarly, in the pitch motion, the *IAE* decreases from 581.20 to 35.90, noting improved performance in both the transient and steady-state outcomes. However, during the heave motion, the adaptive PID-RBF control exhibits a higher *IAE* value (102.08) than the adaptive PID (7.07). This suggests that the adaptive neural tuning technique is less effective at capturing vertical dynamics, which are typically more sensitive to external influences and model nonlinearities. From Table 5, the results indicate that the adaptive PID-RBF control method achieved a significant reduction in tracking error, especially for the two ship motions (surge and pitch). The outcomes for the *DRR* metric are to increase the resilience of the proposed control technique under adverse environmental conditions. For ship surge motion, the suggested Adaptive PID-RBF controller yields results equivalent to the standard adaptive PID, reducing the DRR metric from 0.0987 to 0.0013. These outcomes prove a notably greater ability to reduce perturbation influence than the tracking error rate. A related enhancement is observed in pitch motion, where the DRR decreased from 0.0236 to 0.0025, indicating increased robustness in nonlinear dynamics. However, a ship heave motion indicates a less noticeable enhancement, showing that this direction is still more sensitive to outside perturbations than the two ship surge and pitch motions. Still, the overall system performance remains steady and controlled across three ship motion types. The adaptive PID achieves a lower *DRR* value (0.0001) compared to the adaptive PID-RBF control (0.0010), indicating slightly better normalized disturbance rejection in this axis.

The proposed Adaptive PID-RBF control demonstrates superior robustness to external disturbances, achieving significantly lower *IAE* and *DRR* values across most motion channels compared to adaptive PID control. Although a slight degradation is observed in the second motion type (Heave), the overall performance indicates enhanced disturbance rejection capability. Furthermore, the reduced control energy and bounded error response confirm improved efficiency and closed-loop stability.

5. Conclusions

In this study, an adaptive PID-RBF controller for ship motion control was proposed. The control scheme integrates adaptive PID with the learning adaptation of Artificial Neural Networks based on radial basis functions. To cope with nonlinear dynamics and external disturbances, the controller dynamically adjusted its parameters in real time. Based on simulated results, the efficiency, in terms of control effort, and the tracking error, in terms of accuracy, were considerably improved if compared to adaptive PID control. In addition, the proposed controller had better disturbance rejection capability than the conventional method. Moreover, smoother and better actuation performance, with improved transient characteristics, were achieved with the proposed adaptive PID-RBF controller. All these issues demonstrated that the proposed adaptive PID-RBF controller is a good solution for complex systems like ship dynamics.

Acknowledgment

The authors gratefully acknowledge the College of Artificial Intelligence Engineering, University of Technology-Iraq, Baghdad, Iraq, for their support and assistance during this research.

References

[1] N. M. Noaman, A.S. Gatea, A. J. Humaidi, S.K. Kadhim, A.F. Hasan, "Optimal Tuning of PID-Controlled Magnetic Bearing System for Tracking Control of Pump Impeller in Artificial Heart," Journal Européen des Systèmes Automatisés, vol. 56, no. 1, pp. 21-27, 2023. DOI: https://doi.org/10.18280/jesa.560103.

[2] A.J. Humaidi, A. A. Oglah, S. J. Abbas, I. K. Ibraheem, "Optimal Augmented Linear and Nonlinear PD Control Design for Parallel Robot Based on PSO Tuner," International Review on Modelling and Simulations (I.RE.MO.S.), vol.12, no. 5, pp. 281-291, 2019. DOI: 10.15866/iremos.v12i5.16298

[3] A.F. Hasan, N. Al-Shamaa, S.S. Husain, A.J. Humaidi, A. Al-Dujaili, A., "Spotted Hyena Optimizer enhances the performance of Fractional-Order PD controller for Tri-copter drone," International Review of Applied Sciences and Engineering, vol. 15, no. 1., pp. 82–94, 2024, DOI: https://doi.org/10.1556/1848.2023.00659

[4] N. S. Mahmood, A.J. Humaidi, R.S. Al-Azzawi, "Nonlinear PD State Feedback Control for Electronic Throttle Valve Based on Ant Colony Optimization," 2023 IEEE 11th Conference on Systems, Process and Control, ICSPC 2023 - Proceedings, pp. 38–43, 2023. DOI: 10.1109/ICSPC59664.2023.10420124.

[5] A.F.A. Ahmed, I.M. Elzein, M.M. Mahmoud, S.A.E.M. Ardjoun, A.M. Ewias, and U. Khaled, "Optimal Controller Design of Crowbar System for DFIG-based WT: Applications of Gravitational Search Algorithm," Buletin Ilmiah Sarjana Teknik Elektro, vol. 7, no. 2, pp.122-136, 2025. DOI:10.12928/biste.v7i2.13027.

[6] R.D. Hendriyanto, R.D. Puriyanto, A. Ma'arif, M.A.M Vera, O.I.A. Nugroho, and C. Chivon, "Control of Water Flow Rate in a Tank Using the Integral State Feedback Based on Arduino Uno," Control Systems and Optimization Letters, vol. 2, no. 3, pp.357-365, 2024. DOI:10.59247/csol.v2i3.162.

[7] S.M. Mahdi, A.I. Abdulkareem, A.J. Humaidi, "Improved Tracking Accuracy of Par-4 Delta Parallel Robot Using Optimized FOPID Control with PSO Technique," Journal of Robotics and Control JRC, vol. 6, no. 4, pp. 1721–1728, 2025. DOI:10.18196/jrc.v6i4.26607.

[8] H. Mohammed, B. Midhat, and F. Raheem, "PID and Fuzzy Logic Controller Design for Balancing Robot Stabilization," Iraqi Journal of Computers, Communications, Control and Systems Engineering, vol. 18, no. 1, pp. 1-10, 2018.

[9] N. Thongpance, P. Chotikunnan, A. Wongkamhang, R. Chotikunnan, P. Imura, W. Khotakham, A. Nirapai, and K. Roongprasert, "Comparative Analysis of PID Tuning Methods for Speed Control in Mecanum-Wheel Electric Wheelchairs," Buletin Ilmiah Sarjana Teknik Elektro, vol. 7, no. 2, pp.95-110, 2025. DOI:10.12928/biste.v7i2.13046.

[10] A.F. Hasan, F.A. Raheem, A.J. Humaidi, "Improving Pressure Control in Artificial Ventilation Systems Using a Neural Network-Based Adaptive PID Controller," Automation, vol.7, no. 2, p.37, 2026. DOI: 10.3390/automation7020037.

[11] A. Al-Jodah, S.J.Abbas, A.F. Hasan, A.J. Humaidi, A.S.M. Al-Obaidi, A.A. AL-Qassar, and R.F. Hassan, "PSO-based optimized neural network PID control approach for a four wheeled omnidirectional mobile robot," International Review of Applied Sciences and Engineering, vol. 14, no. 1, pp. 58–67, 2023. DOI:10.1556/1848.2022.00420

[12] N. A. Al-Awad, I. K. Abboud, and M. F. Al-Rawi, "Genetic Algorithm-PID Controller for Model Order Reduction Pantograph catenary System", Applied Computer Science, vol.17, no. 2, pp. 28–39, 2021. DOI:10.35784/acs-2021-11

[13] T. Dlabač, M. Ćalasan, M. Krčum and N. Marvučić, "PSO-based PID Controller Design for Ship Course-Keeping Autopilot," Brodogradnja: An International Journal of Naval Architecture and Ocean Engineering for Research and Development, vol. 70, no. 4, pp. 1-15, 2019. DOI: 10.21278/brod70401.

[14] V. Nicolau, "On PID Controller Design by Combining Pole Placement Technique with Symmetrical Optimum Criterion," Mathematical 354 Problems in Engineering, vol. 2013, no. 1, p316827, 2013. DOI:10.1155/2013/316827

[15] K. J. Åström and T. Hägglund, "Advanced PID Control," ISA, 2006. DOI:10.1002/9781394442102.

[16] Z. Zhiping and Z. Qiang, "Adaptive Self-Regulation PID Tracking Control for the Ship Course," Chinese Journal of Ship Research, vol. 14, no. 3, pp. 145-151, 2019. DOI: 10.19693/j.issn.1673-3185.01305.

[17] Q. Zhang, Z. Ding, and M. Zhang, "Adaptive Self-Regulation PID Control of Course-Keeping for Ships," Polish Maritime Research, vol. 27, no. 1, pp. 39-45, 2020. DOI:10.2478/pomr-2020-0004.

[18] F.G. Martins and M.A. Coelho, "Application of Feedforward Artificial Neural Networks to Improve Process Control of PID-based Control Algorithms," Computers and Chemical Engineering, vol. 24, no. (2-7), pp. 853-858, 2000. DOI:10.1016/S0098-1354(00)00339-2.

[19] J. Rivera-Mejía , A. G Léon-Rubio, and E. Arzabala-Contreras, "PID based on a Single Artificial Neural Network Algorithm for Intelligent Sensors," Journal of applied research and technology, vol. 10, no .2, pp. 262-282, 2012. DOI:10.22201/icat.16656423.2012.10.2.417.

[20] G. De Masi, F. Gaggiotti, R. Bruschi and M. Venturi, "Ship motion prediction by radial basis neural networks," 2011 IEEE Workshop On Hybrid Intelligent Models and Applications, Paris, France, 2011, pp. 28-32, DOI: 10.1109/HIMA.2011.5953967.

[21] M.Y. Hasan, D.J. Kadhim, and A.J. Humaidi, "Prediction of Electricity-Consumption and Residential Bills based on Artificial Neural

Network," International Review of Applied Sciences and Engineering, vol. 16, no. 1, pp.142-152, 2025. DOI: 10.1556/1848.2024.00856
[22] L. Zhang, S. Li, Y. Xue, H. Zhou and Z. Ren, "Neural Network PID Control for Combustion Instability," Combustion Theory and Modelling, vol. 26, no, 2, pp. 383-398, 2022. DOI:10.1080/13647830.2022.2025908.
[23] M.C. Fang, Y. Z. Zhuo, and Z. Y. Lee, "The application of the self-tuning neural network PID controller on the ship roll reduction in random waves," Ocean Engineering, vol. 37, no.7, pp.529-538, DOI: 10.1016/j.oceaneng.2010.02.013.
[24] J. Yu, R. Bu and L. Li, "Ship RBF Artificial Neural Network Sliding Mode PID Heading Control," In MATEC Web of Conferences, vol. 355, p. 03064, 2022, DOI: 10.1051/matecconf/202235503064.
[25] M. H. Enad, R.F. Hassan, A.A. Khaleel Mahmoud, and A.J. Humaidi, "Performance Evaluation of a 2DOF_PID Controller Using Metaheuristic Optimization Algorithms," Journal Europeen Des Systemes Automatises, vol. 57, no. 3, pp. 709–715, 2024. DOI:10.18280/jesa.570308.
[26] A.A. Hassan, N.K. Al-Shamaa, and K.K. Abdalla, "Comparative Study for DC Motor Speed Control using PID Controller," International Journal of Engineering and Technology, vol. 9, no. 6, pp.4181-4192, 2017. DOI:10.21817/ijet/2017/v9i6/170906069
[27] N. Setiawan, W. Caesarendra, and R. Majdoubi, "Implementation of Kalman Filter on PID Control System for DC Motor Under Noisy Condition", Buletin Ilmiah Sarjana Teknik Elektro, vol. 6, no. 3, pp. 271–280, 2024. DOI:10.12928/biste.v6i3.11236.
[28] A.G. Alexandrov, and M.V. Palenov, "Adaptive PID Controllers: State of the Art and Development Prospects," Automation and Remote Control, vol. 75, pp. 188-199, 2014. DOI: 10.1134/S0005117914020027.
[29] L. Xiao, "Parameter Tuning of PID Controller for Beer Filling Machine Liquid Level Control Based on Improved Genetic Algorithm," Computational Intelligence and Neuroscience, 7287796, pp. 1-10, DOI: 10.1155/2021/7287796.
[30] G.A. Ibraheem, A.T. Azar, I.K. Ibraheem and A.J. Humaidi, "A Novel Design of a Neural Network-Based Fractional PID Controller for Mobile Robots Using Hybridized Fruit Fly and Particle Swarm Optimization," Complexity, 3067024, pp. 1-18, 2020, DOI:10.1155/2020/3067024.
[31] L.T. Rasheed, "An Optimal Modified Elman-PID Neural Controller Design for DC/DC Boost Converter Model," Journal of Engineering Science and Technology, vol. 18, no. 2, pp.880-901, 2023.
[32] S. Z. Oleiwi, H.Z. Khaleel, R. Z. Khaleel, M.M. Msallam, A.J. Humaidi, "Smart IoT Irrigation System Using PID-PSO Optimization Method," Advances in Technology Innovation, vol. 11, no. 1, pp. 70–78, 2026, DOI: 10.46604/aiti.2026.15357.
[33] D. Ma and J. Li, "Dynamic Modelling and Optimization of an Eight Bar Stamping Mechanism based on RBF Artificial Neural Network PID control," Frontiers in Mechanical Engineering, VOL. 10, 1374491, 2024. DOI: 10.3389/fmech.2024.1374491.
[34] K. Dileep, S.J. Mija and N.K. Arun, "Radial Basis Function Artificial Neural Network Based PID Tuning for Trajectory Tracking in Robot Manipulator," In 2024 15th International Conference on Computing Communication and Networking Technologies (ICCCNT), pp. 1-7, 2024. DOI:10.1109/ICCCNT61001.2024.10726062
[35] S. J. Kim, M. Jin and J. H. Suh, "A Study on the Design of Error-based Adaptive Robust RBF Artificial Neural Network Back-Stepping Controller for 2-DOF Snake Robot's Head, " IEEE Access, vol. 11, 2023. DOI:10.1109/ACCESS.2023.3249346
[36] C. Kalu, B.U.A. Stephen and M.C. Uko, "Empirical Valuation of Multi-Parameters and RMSE-based Tuning Approaches for the Basic and Extended Stanford University Interim (SUI) Propagation Models," Mathematical and Software Engineering, vol. 3, no. 1, pp.1-12, 2017.
[37] M.Y. Hasan, A.S. Alaraji, A.J. Humaidi, and H. Al-Khazraji, "Adaptive Filtered-x Least Mean Square Algorithm to Improve the Performance of Multi-Channel Noise Control Systems," Mathematical and Computational Applications, vol. 30, no. 4, p.84, 2025, DOI:10.3390/mca30040084.